

# News on Strangeness at Ultrarelativistic Energies - Review of Microscopic Models

Sven Soff<sup>1,2§</sup>

<sup>1</sup> Nuclear Science Division 70-319, Lawrence Berkeley National Laboratory, One Cyclotron Road, Berkeley, CA94720, USA

<sup>2</sup> Institut für Theoretische Physik, Goethe-Universität, Postfach 111932, 60054 Frankfurt am Main, Germany

**Abstract.** We review recent developments in the field of microscopic transport model calculations for ultrarelativistic heavy ion collisions. In particular, we focus on the strangeness production, for example, the  $\phi$ -meson and its role as a messenger of the early phase of the system evolution. Moreover, we discuss the important effects of the (soft) field properties on the multiparticle system. We outline some current problems of the models as well as possible solutions to them.

## 1. Introduction

The purpose of this overview is to present recent developments in the field of microscopic transport theory for ultrarelativistic heavy ion collisions, that is, for energies at SPS and RHIC. Special emphasis is put on the strangeness production. Moreover, we will particularly focus on the role of the  $\phi$ -meson as well as on the importance of the color field properties on *strange* observables. Furthermore, we will also briefly address the topics baryon transport, excitation functions, multi-particle collisions, initial conditions,  $J/\Psi$  data, and particle interferometry.

## 2. Color Fields

An example of what is meant by the importance of field effects on the dynamics is given by the quark molecular dynamics (qMD) model [1, 2]. It is used to study microscopically the dynamics of colored quarks. The intention is to get an effective description of the non-perturbative, soft gluonic part of QCD. In particular, the hadronization process itself can be described explicitly. The initial quark distributions are obtained, for example, from the UrQMD model. The non-equilibrium dynamics of hadronization and the loss of correlations among quarks can be studied subsequently by qMD. The semi-classical model has a two-body color potential between the (anti)quarks. In addition, one has to define a dynamical hadronization criterion. The quarks interact via a Cornell potential with color matrices. Thus, they carry color, (flavor, spin, and isospin). The simple model Hamiltonian is

$$H = \sum_{i=1}^N \sqrt{p_i^2 + m_i^2} + \frac{1}{2} \sum_{i,j} C_{ij} V(|\mathbf{r}_i - \mathbf{r}_j|)$$

§ ssoff@th.physik.uni-frankfurt.de

where  $N$  are the number of quarks in the system. The potential  $V(r)$  is linearly increasing at large distances (confinement) and has a Coulomb-type behavior at short distances. The Cornell-potential is

$$V(r) = -\frac{3}{4} \frac{\alpha_s}{r} + \kappa r .$$

A further approximation is done by allowing only the *diagonal colorless* gluon exchange, that is, the quarks always keep their color. The color matrix elements  $C_{ij}$  determine the sign and relative strength of the interaction depending on the color combination of the pair (for details see [1]).

The rather simple model is surprisingly able to describe a large amount of experimental data, for example, various particle spectra and ratios. Concerning strangeness, we show here the interesting feature of acquiring net strangeness in the quark phase. According to the idea of the strangeness distillation antistrange quarks hadronize earlier in a baryon rich system. Fig. 1 shows the number of net strange quarks ( $s-\bar{s}$ ) as a function of time for the baryon rich system in central Pb+Pb collisions at 30 AGeV. Values up to approximately 10 are reached depending on the string tension. This indicates the possibility to study hyperon matter, hypernuclei, or even strangelets in these high baryon density collisions around the future GSI energies.

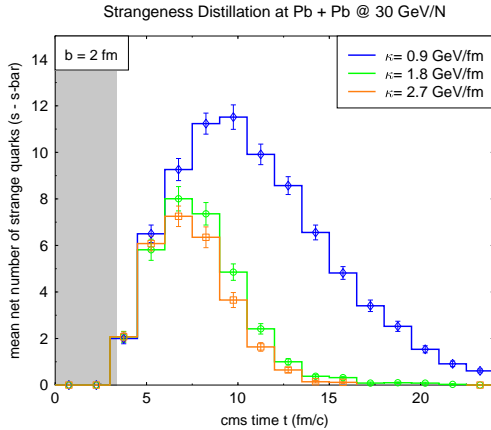


Figure 1: qMD calculation for Pb+Pb at 30 AGeV by S. Scherer [1]. The number of net strange quarks is shown as a function of time for different values of the string tension  $\kappa$ .

Another feature of the model is to study the details of the parton-hadron phase transition that is mainly driven by quark rearrangement. Late stage quark-antiquark pair production is a rather rare process in this model because the strong color fields that are needed are screened. Fig. 2 shows the distribution of the mean path length of quarks before hadronizing. Quarks from the same original hadron (solid line) recluster faster than quarks from different original hadrons (dotted line). The hadron formation follows an exponential decay of the quark cluster to hadrons. The reclustering exhibits a different *decay length* than the rearrangement process (2.2 vs. 4.8 fm). The amount of reclustering ( $\approx 50\%$  for S+Au) demonstrates the survival of correlations in the quark system and possibly incomplete thermalization. This kind of detailed analysis also provides additional insight to the question of the mechanisms of hadronization (recombination vs. fragmentation [3]).

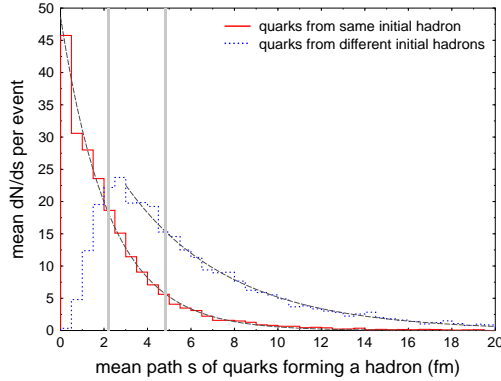


Figure 2: Quark Molecular Dynamics simulation of the hadronization in S(200 AGeV)Au collisions. Quarks originating from the same hadron hadronize after a shorter path length  $s$  than quarks stemming from different hadrons. Figure taken from [1].

### 3. $\phi$ -mesons, baryon transport and the sensitivity to field properties

The field properties also enter in the description of heavy ion collisions by means of cascade calculations that are based on hadron, (di)quark, and string degrees of freedom, as for example the UrQMD model [4]. Here the initial particle production is dominated by string excitations and fragmentations, that is, longitudinally excited color flux tubes. In a dense colored medium the color field strength might be considerably enhanced. The particle formation process in hadronic collisions can be viewed as quantum tunneling of quark-antiquark and gluon pairs in the presence of a background color electric field. It is formed between two receding hadrons which are color charged by the exchange of soft gluons while colliding. In nucleus-nucleus collisions the color charges may be considerably greater than in nucleon-nucleon collisions due to the almost simultaneous interaction of several participating nucleons. With increasing energy of the target and projectile the number and density of strings grows, so that they start overlapping, forming clusters, which act as new effective sources for particle production [5, 6]. It has been predicted that the multiplicities of, for example, strange baryons or antibaryons should be strongly enhanced [6, 8] once the color field strength grows. The abundances of (multiply) strange (anti)baryons in central Pb+Pb collisions at Cern-SPS [7], for example, can only be explained within the framework of microscopic model calculations [8] if the elementary production probability of  $s\bar{s}$  pairs, which is governed in the string models [9] by the Schwinger mechanism [10]  $\sim \exp(-\pi m_q^2/2\kappa)$ , is considerably enhanced. This corresponds either to a dramatic enhancement of the string tension  $\kappa$  (from the default  $\sim 1$  GeV/fm to 3 GeV/fm) or to quark masses  $m_q$  that are reduced from their constituent quark values to current quark values as motivated by chiral symmetry restoration. In a fully analog way,  $\bar{p}$  abundances can be explained since an enhanced string tension similarly leads to an increased production probability of antiquark-diquark pairs which is needed to account for the experimentally observed yields [11]. However, this argument, providing additional motivation, has to be reconsidered if multifusion processes [12], e.g.,  $5\pi \rightarrow \bar{B}B$ , that are neglected in microscopic transport models based on  $2 \rightarrow n$  scatterings, contribute significantly to the baryon pair production. A variation of the string tension from  $\kappa = 1$  GeV/fm to 3 GeV/fm increases the pair production probability of strange quarks (compared to light quarks) from  $\gamma_s = P(s\bar{s})/P(q\bar{q}) = 0.37$  to 0.72. Similarly, the diquark production probability is enhanced from  $\gamma_{qq} = P(qq\bar{q}\bar{q})/P(q\bar{q}) = 0.093$  to 0.45. In general, heavier flavors or

diquarks ( $Q$ ) are suppressed according to the Schwinger formula [10] by

$$\gamma_Q = \frac{P(Q\bar{Q})}{P(q\bar{q})} = \exp\left(-\frac{\pi(m_Q^2 - m_q^2)}{2\kappa}\right).$$

The effectively enhanced string tension in a densely colored environment also follows from its relation to the Regge slope  $\alpha'$ . In the rotational string picture the string tension  $\kappa$  is related to the Regge slope  $\alpha'$  by [13, 14]

$$\kappa = \frac{1}{2\pi\alpha'}.$$

The empirical value of the Regge slope for baryons is  $\alpha' \approx 1 \text{ GeV}^{-2}$  [15] that yields a string tension of approximately 1 GeV/fm. However, high-energetic processes dominated by Pomeron exchange, characterizing the multi-gluon exchange processes existent in high-energetic nucleus nucleus collisions, are described by a Regge trajectory (Pomeron) with a smaller slope of  $\alpha'_P \approx 0.4 \text{ GeV}^{-2}$  [16, 17]. According to Eq. (3) this translates into a considerably larger (*effective*) string tension  $\kappa$ .

Strong color fields also have an impact on the formation times of newly produced (di)quarks and thus on collision rates. The formation times are inversely proportional to the string tension

$$t_f \sim 1/\kappa.$$

The larger the string tension the shorter and short-living are the strings with a certain total energy.

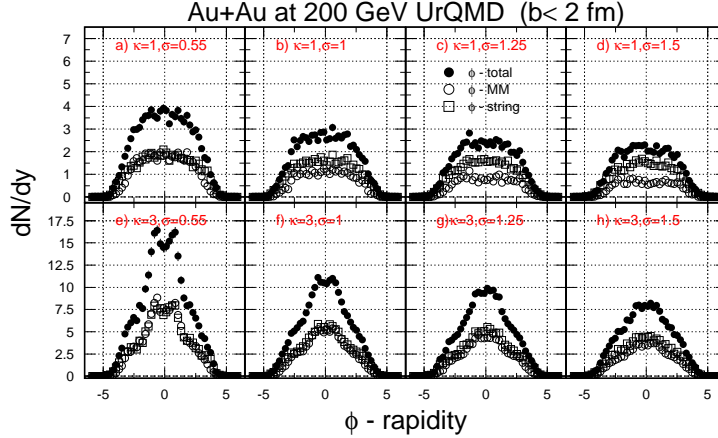


Figure 3: Rapidity distributions of  $\phi$ -mesons in central Au+Au collisions at RHIC. Besides the distributions of all  $\phi$ 's (full circles), the contributions from  $\phi$ 's produced in (resonant) meson-meson ( $K\bar{K}$ ) collisions (open circles) and from  $\phi$ 's originating from string decays (open squares) are shown. Each panel corresponds to different values of the string tension ( $\kappa$ ) (mass term) and the intrinsic transverse momentum broadening parameter  $\sigma$ .

Moreover, Schwinger's formula does not only apply to the mass term but to the transverse momentum term, too. While  $\kappa$  determines the production probability, the intrinsic transverse momentum parameter  $\sigma$  defines the transverse momentum scale. The vacuum value of 0.55 GeV/c (width of a Gaussian) may be considerably enhanced by the strong color fields. Here, we vary both parameters independently to study systematically their individual effects on the observables [18]. Fig. 3 shows

the rapidity spectra of  $\phi$ -mesons at RHIC. The intrinsic  $p_t$  is varied from 0.55 to 1.5 GeV/c (left to right). The upper and lower panels correspond to the vacuum string tension and the SCF scenario, respectively. Clearly a larger  $\kappa$  value leads to a strongly enhanced  $\phi$  production. Increasing the intrinsic  $p_t$  decreases the  $\phi$ -meson yield. The reason for this becomes immediately clear when looking at the production channels. The production in meson-meson ( $K\bar{K}$ ) collisions gets considerably reduced when  $\sigma$  is enhanced. The coalescence-like production loses due to a growing phase space. The experimental study of the  $\phi$ -meson in both decay channels and the observed differences (due to rescattering effects) at RHIC will help to disentangle the different source contributions and thus enlight the role of strong color fields.

Another observable that has been shown to be highly sensitive to SCFs is the netbaryon number transport. Prior to the collision it is non-vanishing only at beam and target rapidities ( $\Delta y \sim 11$  units for RHIC!). Recent data by the STAR [19], PHOBOS [20], BRAHMS [21], and PHENIX [22] collaborations, show a considerable number of netprotons ( $p - \bar{p}$ ) at midrapidity. and antibaryon-to-baryon ratios smaller than unity.

The calculated anti-baryon-to-baryon ratios at midrapidity are shown in Fig. 4 as a function of the strangeness content  $|S|$ , both for  $\kappa = 1$  GeV/fm as well as for the strong color field scenario (SCF,  $\kappa = 3$  GeV/fm) [23]. The  $\bar{B}/B$ -ratios increase with the strangeness content  $|S|$  of the baryons and also increase with with impact parameter  $b$ . There is stronger absorption of antibaryons in central collisions (reducing the numerator of the ratio) and more *stopping* (increasing the denominator). Most important, the  $\bar{B}/B$ -ratios also increase with the color field strength  $\kappa$  what is basically due to an increased pair production (while more collisions should reduce the ratios). The SCF results are closer to data. Also the observed *hyperonization* in the netbaryon distributions supports the SCF scenario (the  $(\Lambda - \bar{\Lambda})/(p - \bar{p})$  ratio is  $\sim 0.8$  for the strong color field (SCF) ( $\kappa = 3$  GeV/fm) scenario, corresponding to the experimental value [22, 19] but smaller for the *vacuum* calculations.

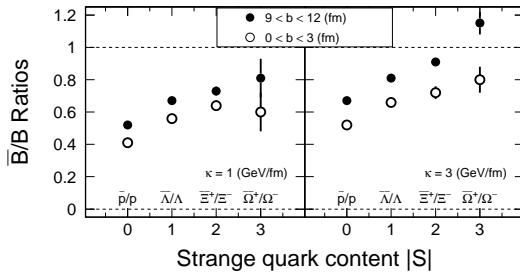


Figure 4: Antibaryon-to-baryon ratios at midrapidity as a function of the strangeness content  $|S|$  in Au+Au collisions at RHIC ( $\sqrt{s_{NN}} = 200$  GeV). Calculations with a string tension of  $\kappa = 1$  GeV/fm are shown on the left and the results with strong color fields ( $\kappa = 3$  GeV/fm) are shown on the right [23].

A complementary or alternative *ansatz* to describe the baryon transport is provided through the parton cascade model (PCM). Fig. 5 shows the netbaryon distributions as calculated with the VNI/BMS version [24, 25] of the parton cascade. It is interesting to note that a considerable fraction of the observed netbaryon number at midrapidity is already contained in the parton distribution functions of the original nuclei. Other contributions arise from secondary scatterings of the partons and fragmentation that together yield a netbaryon number compatible with data. It will be interesting to see whether the correct longitudinal dynamics will also imply the strong transverse expansion dynamics as, for example, the relatively large elliptic flow.

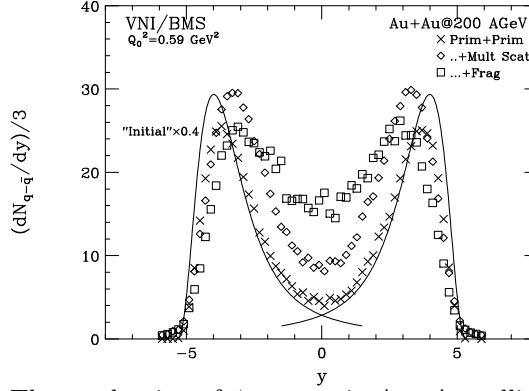


Figure 5: Netbaryon rapidity distributions for Au+Au at RHIC. Crosses are calculation with only primary parton scatterings, rhombes include parton rescattering and squares include rescattering and parton fragmentation. The solid lines show the netbaryon content of the partonic distribution functions for gold nuclei, scaled by an average liberation factor of 0.4. Figure taken from [24].

The production of  $\phi$  mesons in Au+Au collisions at RHIC has also been studied with the quark gluon string model (QGSM) [26]. It is found that the inverse slope parameter agree with data but the absolute yield of  $\phi$ 's is underestimated by a factor 2. Somehow surprising, the fusion of strings does not increase the  $\phi$  yield in QGSM. Similar to previous UrQMD results [8] the early production is governed by string processes. The resonant kaon rescattering production channel dominates in the later stages. Fig. 6 illustrates the freeze-out distribution of the  $\phi$  mesons over rapidity and emission time from QGSM.

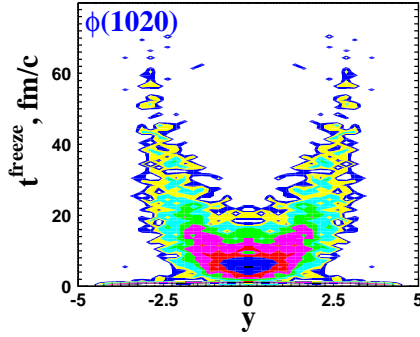


Figure 6:  $d^2N/dydt$  distribution of the final-state  $\phi$  mesons in the  $(y, t)$ -plane from QGSM [26]

The  $\phi$  puzzle has also been addressed with a systematic study of the kaon and dimuon decay channels by the AMPT model [27]. The AMPT model is a multiphase transport model that includes the initial partonic and final hadronic interactions. It starts with minijet partons and strings from the HIJING mode. The partons enter the ZPC parton cascade model. The parton hadron transition is based on the Lund string fragmentation model. Final-state hadronic scatterings are modeled by the ART model. Similar to the other models the resonant  $K\bar{K}$  production channel also contributes considerably to the total  $\phi$  yield. However, even with in-medium modifications of the kaons and  $\phi$ 's the observed differences in the yields cannot be fully explained (see figure 7). An additional ad hoc production is needed to come close to the data (of NA50). It is important to remark that the initial  $\phi$ 's (those that are possibly created through strong color fields) will be primarily visible in the dimuon channel.

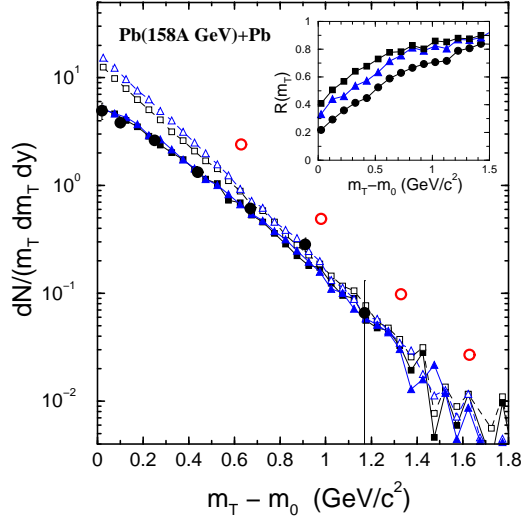


Figure 7: Transverse mass spectra of  $\phi$ 's reconstructed from  $K^+K^-$  pairs (solid symbols) and from  $\mu^+\mu^-$  channel (open symbols) for Pb+Pb at 158A GeV ( $b \leq 3.5$ ,  $|y| < 1$ ) fm in the AMPT model. The results are for without (squares) and with (triangles) in-medium mass modifications. The solid circles are NA49 data [28] for  $\phi \rightarrow K^+K^-$  decay, and the open circles are NA50 data [29] for  $\phi \rightarrow \mu^+\mu^-$ . In the inset is shown as a function of  $m_T$  the ratio  $R(m_T)$  for phi mesons decaying to kaon-antikaon pairs that are not scattered to those determined from the dimuon channel. Circles are for an artificially increased number of  $\phi$ 's by a factor 2 in the HIJING model. Figure from [27].

#### 4. Further Topics

##### 4.1. Excitation functions of meson abundancies and multi-meson fusion

New data from the Cern/SPS allow us to study the excitation function of particle production (and spectra, see [30]) in the interesting energy range of maximum netbaryon densities. Characteristic features in the data as maxima in the  $K^+/\pi^+$  ratio gave reason to speculate about the observation of the phase transition. How do 'conventional' hadron transport theories compare to data [31, 32, 33]? The detailed comparison with two realisations of the cascade model with hadron resonance, (di)quark, and string degrees of freedom (UrQMD and HSD) shows that the kaon yields are described reasonably (see Fig. 8). However, the pion yields and hence the  $K^+/\pi^+$  ratios are off (see figure 9).

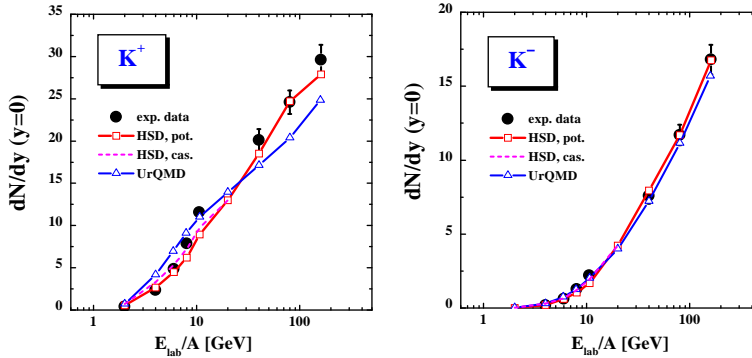


Figure 8: Excitation function of  $K^+$  and  $K^-$  yields from central Au+Au (AGS) or Pb+Pb (SPS) collisions [31] in comparison to experimental data [34, 35].

The overestimation of the pion yields in the model calculations could be due

to a lack of multiparticle back reactions in the model that also lead to 'shorter' chemical equilibration times.  $2 \rightarrow n$  collisions (with  $n > 2$ ) are performed but the inverse channels are not taken care of. Another possible explanation is given through enhanced pion in-medium masses. In fact, the importance of  $3 \leftrightarrow 2$  transitions has been explored in an extended HSD transport approach [36] for antiproton production by meson fusion in  $A + A$  collisions at the AGS and SPS (see figure 10). In order to achieve a more conclusive answer from transport studies multi-particle interactions deserve further investigation in future generations of transport codes.

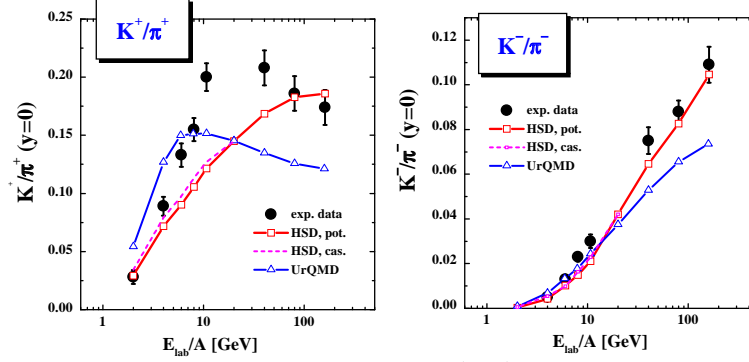


Figure 9: The same as in Fig. 8 for the  $K^+/\pi^+$  and  $K^-/\pi^-$  ratios.

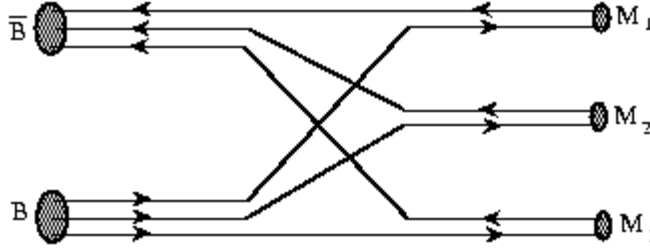


Figure 10: Illustration of the flavor rearrangement model for  $B\bar{B}$  annihilation to 3 mesons and vice versa. The mesons  $M_i$  may be either pseudo-scalar or vector mesons, respectively. Figure from [36]

Within this approach the abundancies of antiprotons as observed from peripheral to central collisions of  $Pb + Pb$  at the SPS and  $Au + Au$  at the AGS can approximately be described.

Fig. 11 shows the reaction rate  $B + \bar{B} \rightarrow mesons$  vs. the backward reaction rate for central Pb+Pb collisions at 160 AGeV. Both rates turn out to be comparable within the statistics demonstrating an approximate local chemical equilibrium. The final  $p$ 's origin dominantly ( $\sim 88\%$ ) from the 3 meson fusion reactions. These studies indicate that these back reactions may have dramatic effects and therefore ask for further investigations.



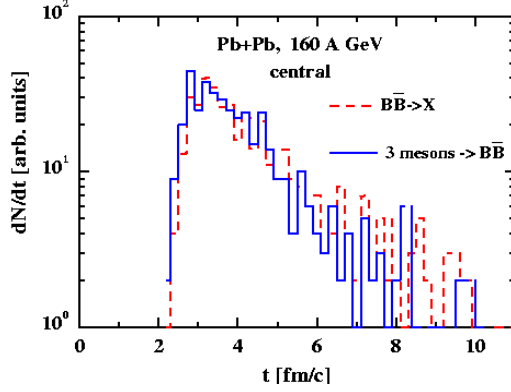


Figure 11: The annihilation rate  $B\bar{B} \rightarrow \text{mesons}$  (dashed histogram) for central  $Pb + Pb$  collisions at 160 A GeV as a function of time in comparison to the backward reaction rate (solid histogram) within the HSD transport approach. Figure from [36].

#### 4.2. $J/\psi$

Another possible QGP signal is charmonium production and its anomalous suppression. It is worth to mention that the new data from NA50 [39], however, do not deviate significantly from the predictions of standard-type cascade calculations (UrQMD or HSD) [37, 38] (Fig. 12). Both the  $E_T$  dependence and the  $E_{ZDC}$  dependence do no longer support the observation of a strong anomalous suppression.

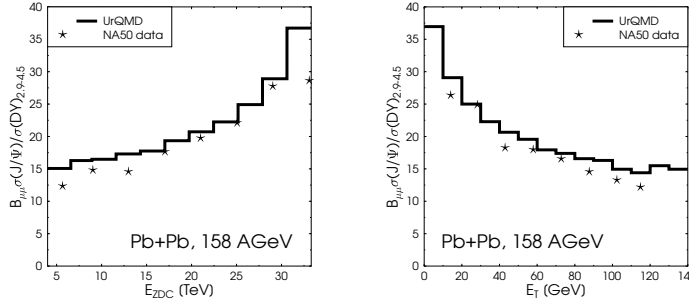


Figure 12: The ratio of  $J/\psi$  to Drell-Yan production as a function of forward energy  $E_{ZDC}$  (left) and transverse energy  $E_T$  (right) for Pb+Pb at 158 A GeV. The preliminary data from the year 2000 NA50 Pb+Pb run [39] are compared to UrQMD results [37]. Figure from [33]

#### 4.3. Initial conditions

The newly developed NEXUS3 model addresses the initial conditions of pp or AA collisions [40, 41]. It provides a self-consistent description of the energy sharing among the participating partons in the collision. The idea is called parton based Gribov-Regge theory, that is, soft and hard processes are described by (multi-)pomeron exchange. As one consequence strings are not necessarily attached to the valence quarks but may be connected to sea quarks. An observable supporting this picture may be given by the  $\bar{\Omega}/\Omega$  ratio in pp collisions which is smaller or close to unity for NEXUS3 but larger for standard string models (or the older versions of NEXUS) [42].

#### 4.4. Particle interferometry

In brief, progress has been made at several frontiers. More realistic models were developed and used to calculate the multidimensional correlation functions. Hybrid-type models, for example, that allow one to study explicitly the sensitivities to the QCD equation of state by simultaneously describing the freeze-out in a realistic way were used to discuss the so-called RHIC HBT-puzzle. The impact of in-medium modifications on HBT results were discussed for the first time. For a discussion and references, see for example [43, 44, 45].

### 5. Outlook

Topics not discussed here are, for example, the necessary tests of the microscopic models by simulating infinite matter. The upcoming RHIC pA data will put severe constraints for the models. An exact understanding of the elliptic flow  $v_2$  is needed (collision numbers, formation times). How is the (partially) hydrodynamic behavior realized on a microscopic level? Also, there has been quite some progress in the charm sector, for example, the prediction of a substantial production of  $J/\Psi$ 's in  $D\bar{D}$  collisions [46], in analogy to the  $\phi$  production via  $K\bar{K}$  [8].

### 6. Summary

Here, we focused on the role of strong color fields that lead to (i) enhanced heavy flavor and diquark production probabilities, (ii) modified, shorter formation times, (iii) stronger intrinsic transverse momenta. The effects on the  $\phi$  meson include (a) enhanced yields, (b) a change of the composition of the spectra, (c) a hardening of the spectra, (d) modified baryon dynamics (hyperonization). Moreover, we briefly discussed the competition of late stage vs. early production and the rescattering of the decay daughters. The differences between the kaonic and muonic  $\phi$ -mesons are desired!

The quark molecular dynamics model provides a (simple) dynamical description of the hadronization process in the soft regime and needs to be further tested.

Parton cascades are now technically established and provide a valuable tool to learn about the validity range of pQCD or necessary modifications.

The study of excitation functions was shown to be essential to detect deficiencies in the models. Additional new developments include the investigation of multi-particle collisions, of charm in microscopic models, and the formulation of the initial conditions in a field theoretical language (parton ladders).

### Acknowledgments

This work was supported by the Alexander von Humboldt-Foundation through a Feodor Lynen Fellowship, BMBF, DFG, GSI, and NSF grant PHY-03-11859. We thank S. Kesavan, V. Koch, J. Randrup, S. Scherer, H. Stöcker, and N. Xu, for many helpful comments and/or for providing figures.

### References

- [1] Scherer S, Hofmann M, Bleicher M, Neise L, Stöcker H, Greiner W 2001 *New J. Phys.* **3** 8
- [2] Hofmann M, Scherer S, Bleicher M, Neise L, Stöcker H, Greiner W 2000 *Phys. Lett. B* **478** 161
- [3] R. J. Fries, B. Müller, C. Nonaka and S. A. Bass, arXiv:nucl-th/0305079.
- [4] Bass S A *et al.* 1998 *Prog. Part. Nucl. Phys.* **41** 255.
- [5] T. S. Biro, H. B. Nielsen, J. Knoll, Nucl. Phys. **B245**, 449 (1984).

- [6] H. Sorge, M. Berenguer, H. Stöcker, W. Greiner, Phys. Lett. B **289**, 6 (1992). N. S. Amelin, M. A. Braun, C. Pajares, Phys. Lett. B **306**, 312 (1993). H. Sorge, Nucl. Phys. A **630**, 522 (1998).
- [7] E. Andersen *et al.* [WA97 Collaboration], Phys. Lett. B **433**, 209 (1998).
- [8] S. Soff *et al.*, Phys. Lett. B **471**, 89 (1999); S. Soff *et al.*, J. Phys. G **27**, 449 (2001).
- [9] B. Andersson, G. Gustafson, G. Ingelman, T. Sjöstrand, Phys. Rept. **97**, 31 (1983).
- [10] J. S. Schwinger, Phys. Rev. **82**, 664 (1951).
- [11] M. Bleicher *et al.*, Phys. Lett. B **485**, 133 (2000).
- [12] R. Rapp, E. Shuryak, Phys. Rev. Lett. **86**, 2980 (2001); C. Greiner, S. Leupold, J. Phys. G **27**, L95 (2001).
- [13] P. Goddard, J. Goldstone, C. Rebbi, C. B. Thorn, Nucl. Phys. B **56**, 109 (1973); K. Johnson, C. B. Thorn, Phys. Rev. D **13**, 1934 (1976).
- [14] C. Y. Wong, *Introduction To High-Energy Heavy Ion Collisions*, World Scientific, Singapore (1994), 516 p.
- [15] M. B. Green, Phys. Scripta **T15**, 7 (1987).
- [16] G. Veneziano, Phys. Rept. **9**, 199 (1974).
- [17] P. D. Collins, *An Introduction To Regge Theory And High-Energy Physics*, Cambridge 1977, 445p.
- [18] S. Soff, S. Kesavan, N. Xu, *et al.*, in preparation.
- [19] C. Adler *et al.* [STAR Collaboration], Phys. Rev. Lett. **87**, 262302 (2001); Phys. Rev. Lett. **86**, 4778 (2001); Phys. Rev. Lett. **89**, 092301 (2002).
- [20] B. B. Back *et al.* [PHOBOS Collaboration], Phys. Rev. Lett. **87**, 102301 (2001).
- [21] I. G. Bearden *et al.* [BRAHMS Collaboration], Phys. Rev. Lett. **87**, 112305 (2001).
- [22] K. Adcox *et al.* [PHENIX Collaboration], Phys. Rev. Lett. **88**, 242301 (2002); Phys. Rev. Lett. **89**, 092302 (2002).
- [23] S. Soff, J. Randrup, H. Stöcker and N. Xu, Phys. Lett. B **551**, 115 (2003).
- [24] S. A. Bass, B. Müller and D. K. Srivastava, arXiv:nucl-th/0212103.
- [25] S. A. Bass, B. Müller and D. K. Srivastava, Phys. Lett. B **551**, 277 (2003).
- [26] L. Bravina, L. Csernai, A. Faessler, C. Fuchs, S. Panitkin, N. Xu and E. Zabrodin, arXiv:hep-ph/0208161.
- [27] S. Pal, C. M. Ko and Z. w. Lin, Nucl. Phys. A **707**, 525 (2002).
- [28] S.V. Afanasiev *et al.*, (NA49 Collaboration), Phys. Lett. B **491** (2000) 59.
- [29] V. Friese, Dissertation (1999), University of Marburg;  
D. Röhrich, J. Phys. G **27** (2001) 355.
- [30] M. Gazdzicki, arXiv:hep-ph/0305176.
- [31] H. Weber, E. L. Bratkovskaya, W. Cassing and H. Stöcker, Phys. Rev. C **67**, 014904 (2003).
- [32] H. Weber, E.L. Bratkovskaya, and H. Stöcker, Phys. Lett. B **545**, 285 (2002).
- [33] M. Reiter, E. L. Bratkovskaya, M. Bleicher, W. Bauer, W. Cassing, H. Weber and H. Stöcker, arXiv:nucl-th/0301067.
- [34] S.V. Afanasiev *et al.* (NA49 Collab.), Phys. Rev. C **66** (2002) 054902.
- [35] L. Ahle *et al.* (E866 and E917 Collab.), Phys. Lett. B **476**, 1 (2000); Phys. Lett. B **490**, 53 (2000).
- [36] W. Cassing, Nucl. Phys. A **700**, 618 (2002).
- [37] C. Spieles, R. Vogt, L. Gerland, S. A. Bass, M. Bleicher, H. Stöcker and W. Greiner, Phys. Rev. C **60**, 054901 (1999).
- [38] W. Cassing and E. L. Bratkovskaya, Nucl. Phys. A **623** (1997) 570.
- [39] L. Ramello, (NA50 Collab.), talk given at QM2002.
- [40] H. J. Drescher, M. Hladik, S. Ostapchenko, T. Pierog and K. Werner, Phys. Rept. **350**, 93 (2001).
- [41] K. Werner, talk given at SQM2003.
- [42] M. Bleicher, F.M. Liu, A. Keranen, J. Aichelin, S.A. Bass, F. Becattini, K. Redlich, K. Werner, Phys. Rev. Lett. **88**, 202501 (2002).
- [43] S. Soff, S. A. Bass, D. H. Hardtke and S. Y. Panitkin, Nucl. Phys. A **715**, 801 (2003).
- [44] Soff S, Bass S A, Hardtke D, Panitkin S 2002 *Phys. Rev. Lett.* **88** 072301
- [45] Soff S, Bass S A, Dumitru A 2001 *Phys. Rev. Lett.* **86** 3981.
- [46] E. L. Bratkovskaya, W. Cassing and H. Stöcker, Phys. Rev. C **67**, 054905 (2003).